Journal of Supramolecular Structure 14:405–422 (1980)

Averages of Glutamine Synthetase Molecules as Obtained With Various Stain and Electron Dose Conditions

M. Kessel, J. Frank, and W. Goldfarb

Division of Laboratories and Research, New York State Department of Health, Albany, New York 12201

Averaged projections of individual glutamine synthetase molecules have been obtained by using electron microscopy and image processing. The methodology of correlation averaging under low dose conditions is described in detail. Because of their low signal-to-noise ratio, images made under low dose conditions cannot be directly interpreted in terms of high resolution features. Computer averaging of these images reveals a division of the subunit projection into two domains whose sizes agree with results of Lei et al [2] limited proteolysis experiments.

Key words: glutamine synthetase, electron microscopy, computer averaging, pattern recognition, radiation damage, low dose

Glutamine synthetase (GS) plays a central and complex role in nitrogen metabolism [1]. It functions both to catalyze the ATP-dependent synthesis of glutamine from ammonia and glutamate and to control the assimilation of nitrogen from various compounds. Its function in the production of glutamine is important since glutamine is the first step of a highly branched metabolic pathway which takes a part in the ultimate synthesis of nearly all the important macromolecules of the cell.

A recent study by Lei et al [2] has shown that trypsin will cleave the 50,000 MW glutamine synthetase subunit into two principal fragments of molecular weights 32,000 and 18,000. The authors conclude that the sites of substrate binding are closely identified with a proteolysis-susceptible region of the glutamine synthetase polypeptide chain. Lei et al [2] suggest, as one of the two models for the GS subunit a two-domain structure, with masses of roughly 32,000 and 18,000 daltons, and the susceptible peptide forming a connection between the domains. The results of the present paper using low dose electron microscopy support this model by showing evidence of a bilobed subunit.

M. Kessel is now at the Hebrew University-Hadassah Medical School, Jerusalem. Reprint requests should be directed to J. Frank, New York State Department of Health, Albany, New York 12201.

Received December 4, 1979; accepted August 11, 1980.

Structural studies of GS have been made by both electron microscopy [3] and x-ray diffraction [4]. The study by Valentine et al [3] showed that the 600,000 MW complex is composed of 12 subunits arranged at the corners of two eclipsed hexagons producing a double layered dodecamer with a hexagonal profile. The complex has a diameter of 140 Å and a height of 60–80 Å. The D_6 symmetry of the GS molecule was also found by Eisenberg et al [15] and Frey et al [6].

Frey [7] studied a polymeric form of GS which forms helical cables of stacked disks when Co^{++} ions are added to a solution of the enzyme. The three-dimensional reconstruction of the cables gives some idea of the bond sites between the disks, and particular z-sections of the reconstruction show the central stack of disks to have a definite subunit handedness.

The most detailed structure of the enzyme by electron microscopy is that published by Frank et al [8, 9], who used averaging techniques to produce a reconstruction based on the average of 50 molecules of negatively stained high dose images. The outstanding feature of the reconstruction is an apparent handedness of the subunits, which most likely arises from only one of the hexamers being contrasted by the stain.

This method utilizes the fact that some kinds of molecules attach themselves to the carbon film of the electron microscope grid in a characteristic orientation. Molecules that make this preferred attachment differ among themselves in horizontal location and one angle of orientation, but have their other two angles of orientation fixed by the carbon film. This allows the use of two-dimensional image correlation techniques to build up a sum of accurately aligned molecular projections.

The multisubunit enzyme glutamine synthetase has this useful property. The overall shape of the molecule is that of a short cylinder made up two eclipsed rings of six subunits [3]. Individual particles tend to rest on one of their flat sides, thus presenting the same view to the electron microscope.

The aim of the present study was to refine the previous analysis [8, 9] by the use of low dose techniques and an alternative staining method. Preliminary reports on this work were given elsewhere [10–12].

MATERIALS AND METHODS

Sample Preparation

Purified GS [13] from E coli was obtained from Professor F. Wedler of Pennsylvania State University. The sample was supplied at a concentration of 20 mg/ml in a buffer of 10 mM imidazole, 5 mM $MnCl_2$ (pH 6.5). The adenylylation state of the enzyme was determined as E_{11}.

Electron Microscopy

Staining. A drop of glutamine synthetase diluted to 170 μg/ml with buffer was applied to a specimen grid coated with a thin carbon film supported by carbon-stabilized collodion nets. The specimen was stained with 1% uranyl formate.

For the glucose/stain preparation, the samples were stained with a solution of 0.15% uranyl acetate and 0.5% glucose.* The two components were mixed immediately prior to staining.

Low dose procedure. Micrographs were recorded at 100 kV using the Philips EM 301. The low dose (~1 electron/$Å^2$) procedure adopted was essentially that of Unwin and Henderson [14] except that the off-axis viewing screen was dispensed with as described by Henderson et al [15].

*This method of embedding was suggested by Dr. Wah Chiuh (1978, personal communication).

A narrow, coherent illuminating beam was produced by using a 20-μm first condenser aperture and a 200-μm second condenser aperture. The first condenser lens was moderately excited at 1.0 A. The beam was prevented from reaching the specimen by means of a fixed displacement of the CI aperture holder rod positioned midway between two apertures. No objective aperture was used. Grids were scanned at X 1,900 at an illumination level of $\sim 2.5 \times 10^{-2}$ e/Å^2/s at the specimen. An anticontamination device was used at all times. When an apparently satisfactory area of the specimen had been selected, a location marker was used either on the left or right-hand specimen drive. The grid was then moved by a distance of about 30 μm. The beam was blocked at the level of the CI aperture holder and the magnification increased to the desired working magnification of $\sim$ X 42,000. The beam stop was removed and the image corrected for astigmation and desired focal setting. The beam was blocked again and the specimen area originally selected was positioned in the middle of the screen by using the predetermined marker. The beam stop was then opened simultaneously with the opening of the camera shutter for a 2s exposure on the photographic emulsion. Immediately following the initial exposure the electron dosage was increased and both a medium dose (40 e/Å^2) and high dose micrograph (400 e/Å^2) recorded without the beam's being blocked between successive exposures.

Micrographs were recorded on Kodak 4489 Electron Image Plates and developed in D-19 for 12 minutes at 20°C for maximum development (Kodak pamphlet no. P-198). Our convention was to place the specimen side of the grid facing the electron beam. Thus micrographs made with the emulsion facing away from the enlarger light present a view of the specimen as though seen through the carbon substrate.

Calibration of the electron dosage. Electron dosages were calibrated with a Faraday cage designed by Turner et al [16] and were considered to be more accurate estimates than those based on the optical density of the plates.

Magnifications were calibrated using the 41 Å spacing between subunit annuli in the tail of bacteriophage T_4 [17].

Micrograph selection. Electron micrographs were selected based on the optical diffraction patterns of the carbon film from the high dose micrograph. Low and medium dose micrographs were of insufficient contrast to produce a perceiveable optical diffraction pattern. Only those micrographs displaying well corrected astigmatism and a amount of defocus appropriate for recording detail down to 10–15 Å with phase contrast of the same sign were selected for further processing.

Image Processing

Computer system. For computing, a Digital Systems PDP 11/45 was used with the DEC RSX 11D executive to run the modular image processing system SPIDER [18]. The computer is equipped with a floating point processor, a 1,600 bpi tape unit, two 170-Mbyte disk units, plotter, line printer, and VERSATEC printer. For interactive image processing operations, a Princeton Electronics storage tube with TV monitor is available.

Digitization of micrographs. Electron micrographs to be processed were digitized with a Perkin-Elmer flatbed microdensitometer PDS 1010A. The sampling distance and scanning aperture were chosen in such a way that adequate representation of the information transferred by the electron microscope is assured.

Alignment methodology. The method to achieve alignment of identical particle views [8, 18, 19] is based on the properties of the auto-correlation function (ACF) and cross-correlation function (CCF) of particle images. The computational steps are summarized in a block diagram (Fig. 1). Low dose images posed some special problems which will de discussed in the results section.

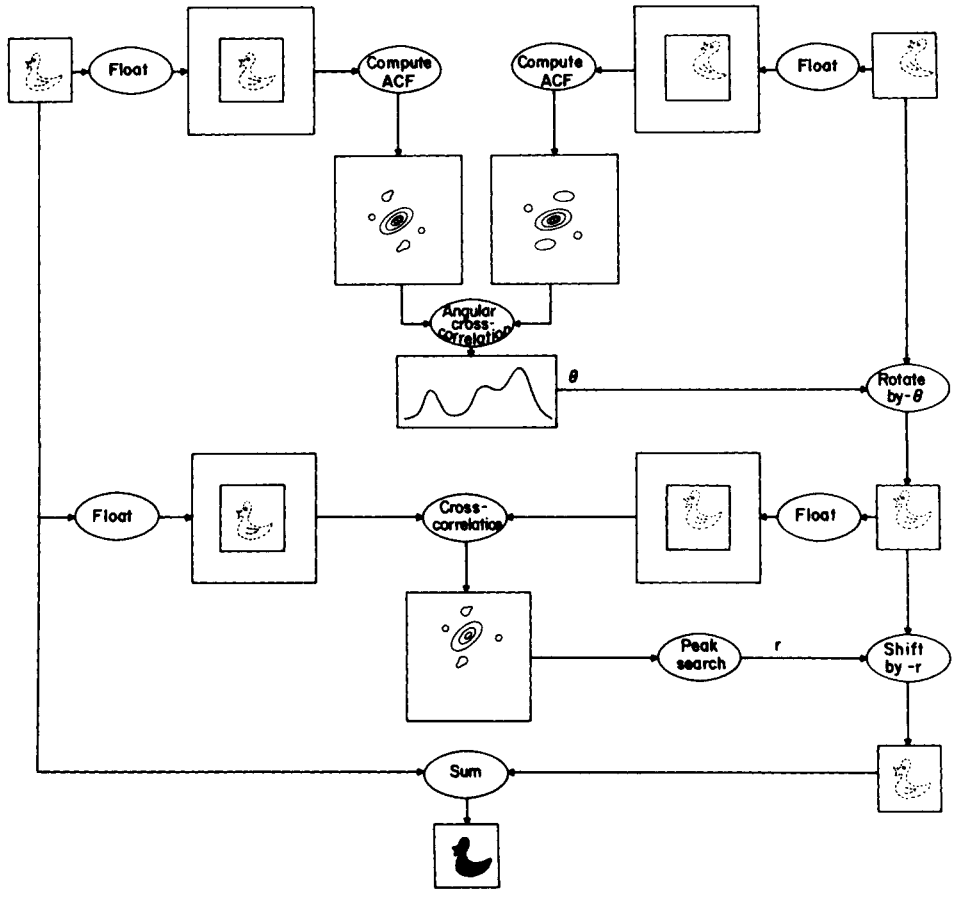

Fig. 1. Block diagram of the alignment algorithm as it is implemented in the computer (adapted from [12], courtesy by Springer-Verlag). The duck on the top right is brought into the same relative position with respect to the image frame as the "reference duck" on the top left. After alignment, the images can be added together (bottom). For determination of the relative orientation, the images are auto-correlated, and the auto-correlation functions are rotated with respect to each other to find the matching position. The result of this search is a series of angular correlation curves (cf Fig. 5), which allow a more detailed analysis to be made. The angle so found is used to rotate the image on the right into the same orientation as the reference image. The relative translation of the rotated image with respect to the reference is then found by computing the cross-correlation function and searching the position of the correlation peak. A subsequent shift operation completes the alignment. Each correlation operation is preceded by the floating of the image, ie, by putting the image into the center of a larger array to avoid artifacts from false overlaps inherent to the Fourier method of computation.

RESULTS

Figure 2 is a general view of a field of negatively stained GS particles from E coli recorded with a conventional electron dose of about 400 e/Å^2. The majority of the enzyme molecules lie on the carbon film in a characteristic orientation with their flat surfaces attached to the plane of the film. In addition, a few molecules are also seen in side view appearing in some cases as stacks of double disks with a 45 Å spacing corre-

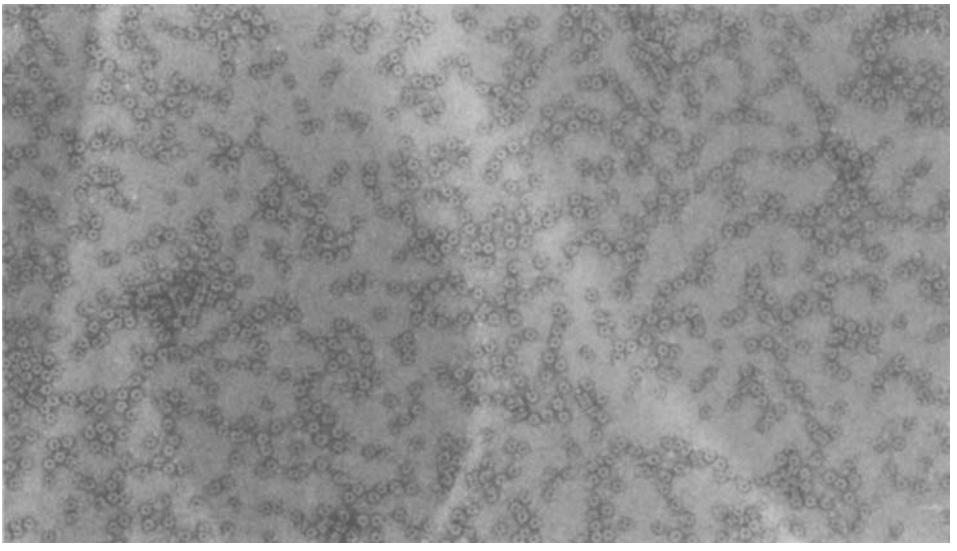

Fig. 2. View of a field of GS molecules on a carbon grid recorded with 400 e/Å^2 and an electron optical magnification of × 42,000.

sponding to the side-on height of a single hexamer. The particles are very similar to those described by Valentine et al [3]. Apart from the hexagonal shape, and some indication of internal hexagonal symmetry, the high dose imaged particles show no clearly defined details in the projection.

The averaging approach is based on the multiple occurrence of a two-dimensional motif in the image. When more than one motif is present, the averaging is still feasible if the different motifs can be clearly distinguished at the selection step.

Theoretically, a cylinder with D6 symmetry lying on one of its two flat faces should present only one view in axial projection, and this view should exhibit six lines of mirror symmetry. From this consideration we expected one view and this was not contradicted by inspection of the micrographs. We had therefore no reason to distinguish between different particle views at the selection step.

Another point of concern was the question of whether the particles are indeed axially projected as required by the averaging method. The angle by which the direction of projection is allowed to deviate from the particle axis is easily calculated: Even if we ignore the flattening and assume a particle height of 80 Å, a resolution of 20 Å would allow for a variation of ± 15° in the projection angle before it would become noticeable.

Three adjacent fields represented by 500 × 700 picture elements were scanned from each micrograph of the dose series. One of these fields is shown in Figure 3 for low (1 e/Å^2), medium (40 3/Å^2), and high (400 e/Å^2) dose conditions.

Selection of the particles and general averaging strategy. Arrays of 64 × 64 image elements each containing one particle and some of its neighborhood are successively selected from the scanned field and put into separate files. This is done by using an inter-

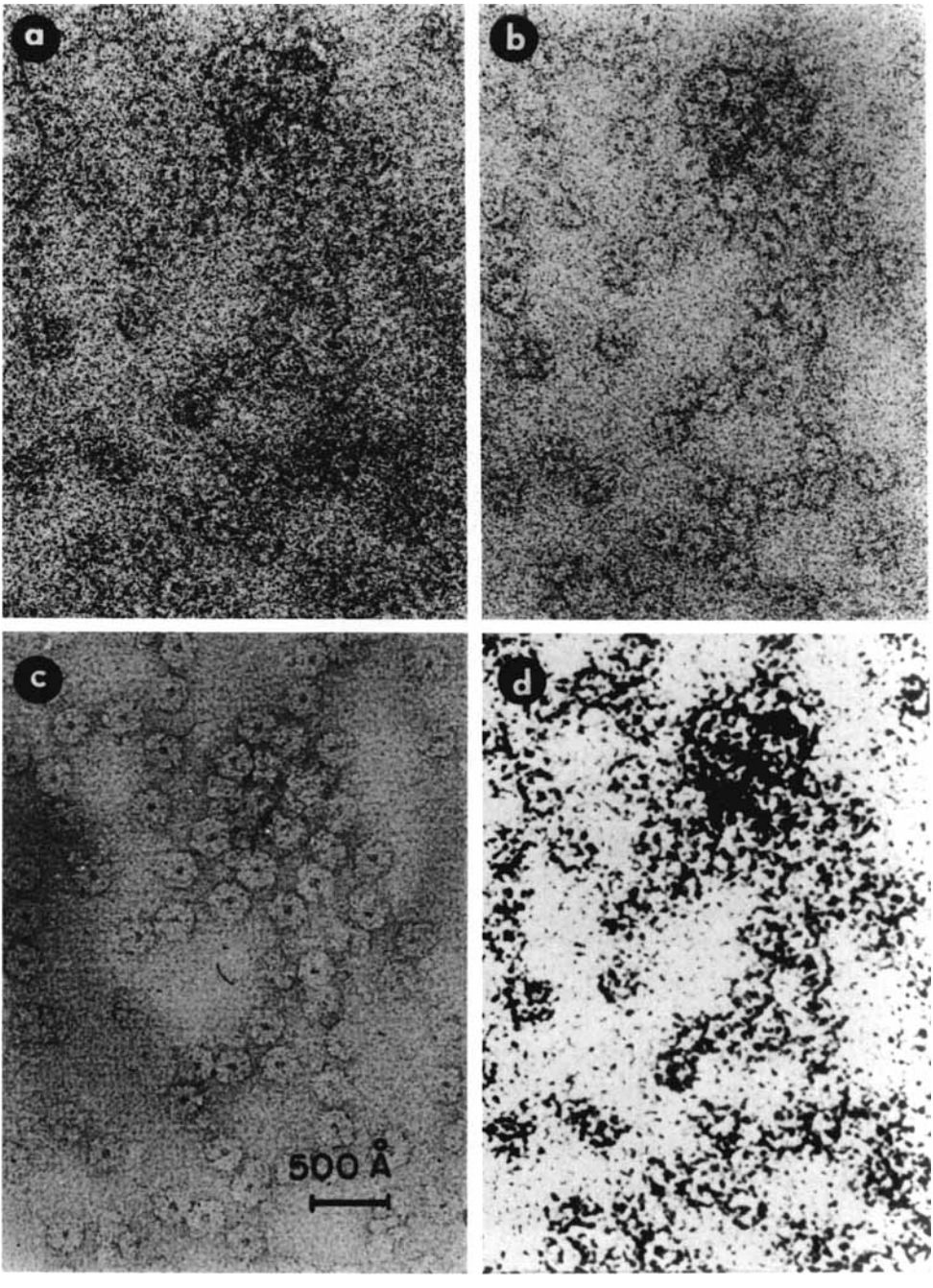

Fig. 3. Scanned arrays containing identical fields of molecules at different doses. These arrays have the dimensions 512 × 700 and are displayed on a computer-linked display device to select molecules for further processing. a) 1 e/Å^2, b) 40 e/Å^2, c) 400 e/Å^2, d) 1 e/Å^2 contrast enhanced.

active selection program that is part of the image processing software system [18, 19]. Only those particles that were well separated on the grid and appeared intact were selected. Interactive selection is possible with low dose electron micrographs of negatively stained preparations only after the particles are made visible on a contrast-enhanced display (Fig. 3) [20]. However, this procedure failed for images from specimens treated with a mixture of glucose and uranyl acetate: The particles that could be identified in the high dose images were no longer visible in the low dose images despite elaborate enhancement attempts. In this case a method of "blind" alignment was used, which is based on the positions of the high dose particles and the correlation between corresponding areas of the support film in high and low dose micrograph. This detail is described below.

In the reconstruction of the low dose particles, we made use of the fact that for each particle, a statistically well-defined high dose image is available, from which the orientation angle and the translation vector with respect to a selected reference particle may be obtained. Since the exposure to electrons primarily affects high resolution features of the molecule structure, these values, although not sufficiently accurate for the corresponding low dose particles' final average, can nevertheless be used as estimates in order to build up a preliminary average. This average could then be used as reference in a subsequent refinement run.

How many particles are needed to form a statistically meaningful average? To obtain an estimate we can assume that the shot noise is the predominant noise source in low dose electron micrographs. According to the Rose equation as applied to electron microscopy [21], approximately

$$n = \frac{25}{c^2 d^2}$$

electrons per unit area are needed to define a detail of size d and contrast c in the image.* If we take $c = 0.05$ as a conservative estimate of the contrast and $d \simeq 15$ Å as the smallest significant detail to be expected with negative stain, we obtain $n \simeq 45$ el/Å^2. This means that for an electron dose of 1 el/Å^2, no more than 45 particles are needed to obtain a statistically significant average.

We used about 50 particles in each reconstruction of the negatively stained molecules. This allowed us to form two partial averages in each case, each average comprised of 25 particles, as a check for reproducibility. The additional sixfold rotational averaging brings the total number of subunits participating in the partial average to 150, and in the total average to 300. In the case of the glucose/stain treated specimens, only 20 particles were used in the final average (ie, 120 including sixfold averaging).

Alignment of negatively stained molecules. A particle was selected for reference (Fig. 4a) which shows six-fold symmetry and an even stain distribution at the periphery. We found that any bias introduced by the selection of the reference is later removed in the refinement run. The typical ACF of the GS particle (Fig. 4b) shows an indication of the six-fold symmetry. Since the GS image shows stain accumulations at the particle periphery which are not necessarily related to the particle structure, not all circles of the ACF contain information relevant to the alignment of the stain-excluding regions. The contributions from several

*For a proper application of the formula and its reconciliation with Unwin and Henderson's formula [14], only that part of the total image contrast should be used that gives rise to a significant signal variation within the distance d. This difference becomes increasingly important as the resolution is increased (ie, d decreased).

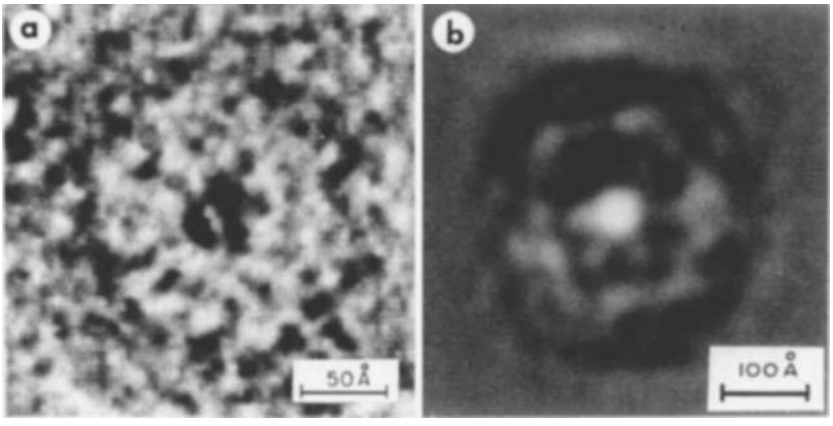

Fig. 4. a. Particle used as reference. A particle is selected that is representative of the inspected particles with regard to size and symmetry. b) Typical auto-correlation function of a GS particle, showing sixfold symmetry.

circles with different radii (Fig. 5) show various degrees of sixfold symmetry, indicated by the presence of three maxima within $-90^\circ < 0 < +90^\circ$. Appropriate weights were used to emphasize the contributions from radii where the sixfold symmetry is strongly expressed.

A section through the CCF (Fig. 6) shows that the total peak width is of the order of 40 Å, which is the correlation distance expected for negatively stained material with a typical resolution of 20 Å. Because of the peak symmetry, the position of the center is defined within at least 1/10 of the total peak width, giving an estimated alignment accuracy of 4 Å.

In all our experiments, the algorithm for orientation search gave unreliable results when applied to low dose data so that the rotation angles had to be "borrowed" from the corresponding high dose set. In contrast, it was possible to make the translational search between low dose negatively stained particles work, by application of a suitable low-pass filter to the cross-correlation function [19]. Because of the "white" Fourier spectrum of Poisson noise, low-pass filtering of quantum noise limited images generally enhances the signal contribution to the correlation integral.

This behavior is implicit in Saxton and Frank's [22] formula in which the electron dose per unit area n, the image contrast c, the sampling distance d, and the particle diameter D are related by

$$n \geqslant \frac{3}{c^2 Dd} .$$

A detectable signal peak will appear in the cross-correlation function if the electron dose is large enough to fulfill this inequality. If this inequality does not hold for a given set of values for n, c, D, and d, it can be fulfilled by increasing the sampling distance d. The coarsening of the sampling grid is equivalent to low-pass filtering. The same effect is automatically achieved when a particle average is used as reference: The averaging effectively eliminates the high resolution noise part of the Fourier spectrum.

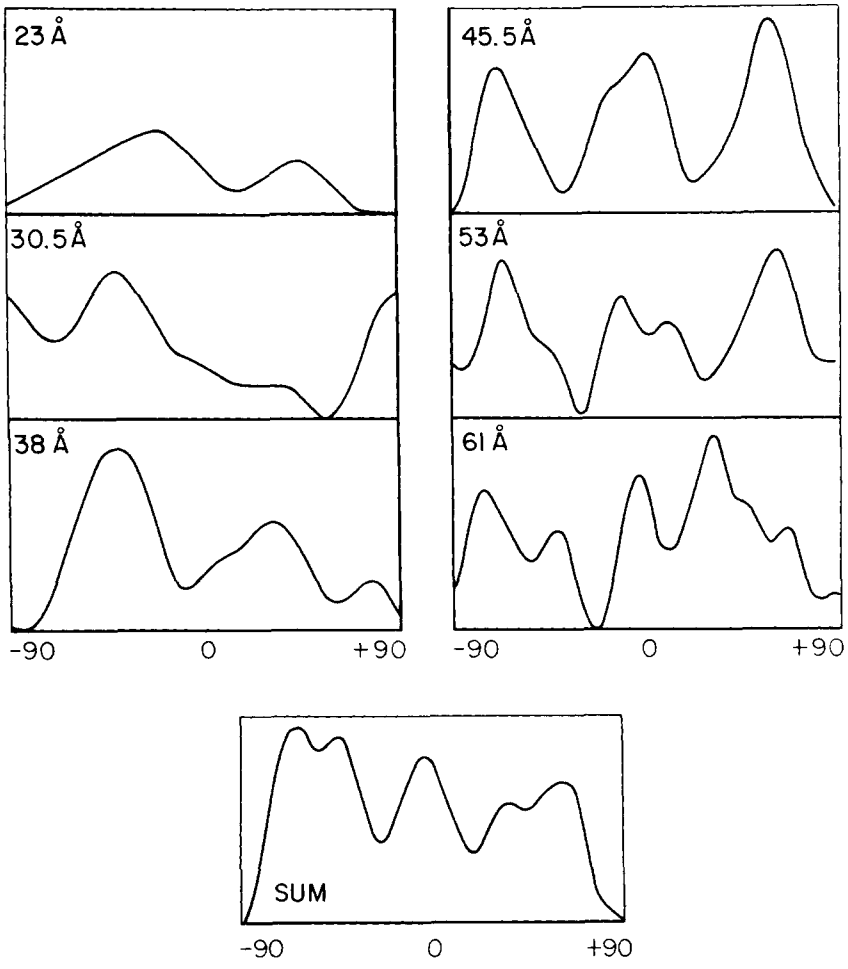

Fig. 5. Angular correlation curves of two glutamine synthetase molecules for different radii of the ACF. The curves differ in their offsets but have a common scaling. Sixfold symmetry is apparent from the three equidistant maxima in the 180° angular correlation range, for radii between 38 Å and 53 Å. The sum curve is obtained by applying equal weights to the contributions from the different ACF radii.

"Blind" alignment method. The molecules are not visible in the low dose micrograph when the glucose/uranyl-acetate mixture was used in the preparation. Here we proceeded in the following way: Rotation angles and translation vectors were obtained from the high dose micrographs, which show the molecules faintly visible. The contrast enhancement technique used in the case of low dose images of negatively stained molecules failed to visualize the glucose/stain prepared particles. In order to pick out the invisible particles for averaging, we relied on the assumption that the particles did not move with respect to the carbon film between low dose and high dose exposure. The low dose particles were picked out from the image by using windows that had the same relative position with respect to the carbon support film as the windows used to pick out the high dose particles. If there is a translation between high dose and low dose

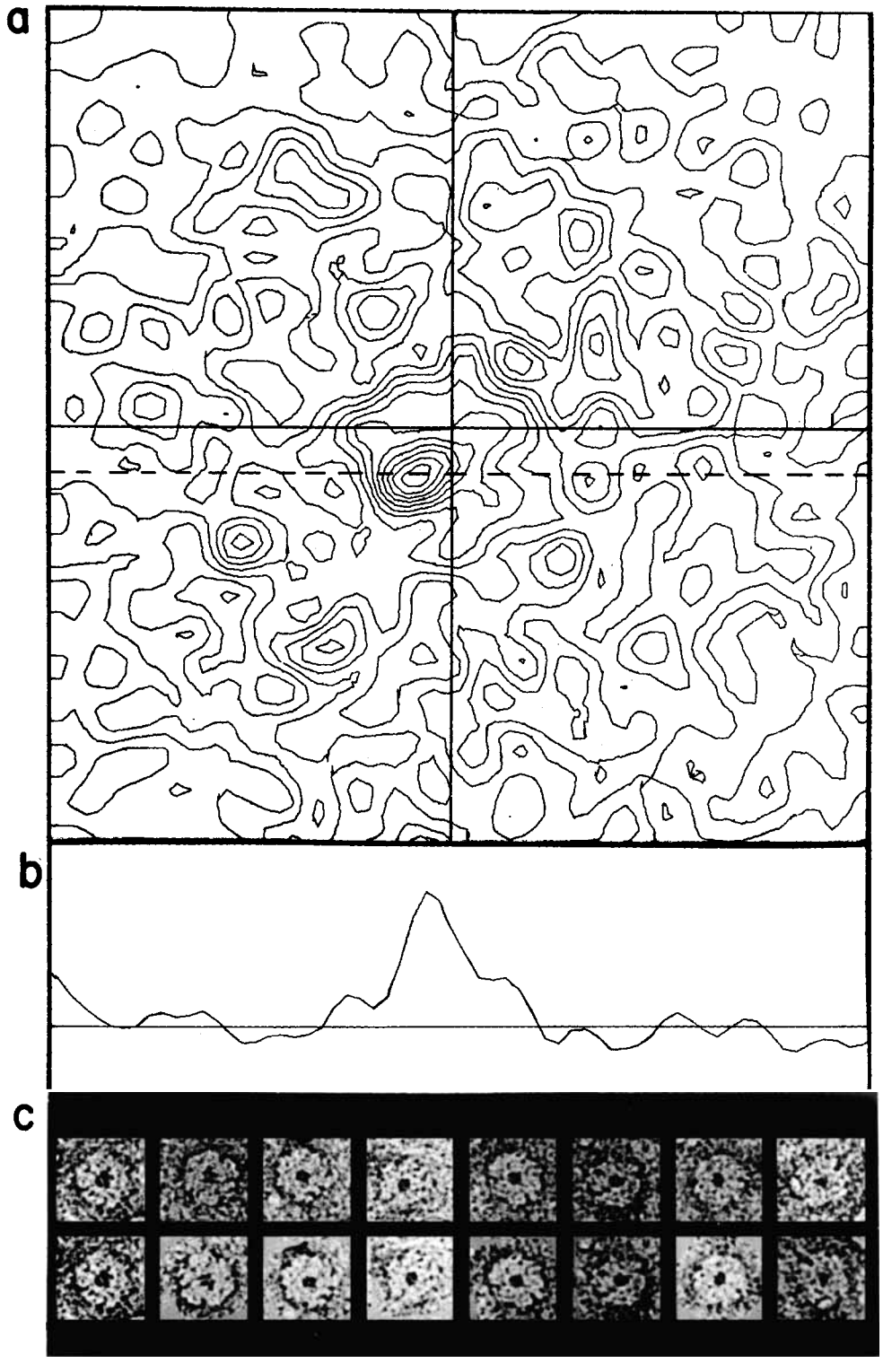
a
b
c

micrographs, the new windows will all be offset from their old counterparts by a common offset vector. If there is an additional rotational misalignment, the offset vector between corresponding windows will vary over the whole micrograph frame according to simple rules of geometry.

We found both translation and rotation between the scanned micrograph areas by using cross-correlation between 256 X 256 arrays in the four corners [23]. The main correlation contribution comes from the carbon support film. The large size of the areas and the use of low-pass filtering made it possible to detect the correlation peak. Within two image elements, all four areas showed identical shifts, indicating the absence of an appreciable rotation between the electron micrographs. The images windowed out were subjected to the rotations and translations found in the high dose set and subsequently averaged. So far we have not found an algorithm sensitive enough to achieve alignment of these images without use of external information.

Averaging. The average of all aligned particles (Fig. 6c) and various subsets of them were formed by simple addition and were displayed using contour maps and the filmwrite option of the microdensitometer. A safeguard was needed to prevent those particles from participating in the average that were not properly aligned by the alogrithm. On visual inspection, the majority of the particles treated by the alignment algorithm appear to be aligned with high precision, whereas some particles are completely off the correct position ("runaway"). Because of imbalanced negative stain accumulation or strong structural distortions, the "true" correlation peak of these particles is outweighed by a noise peak whose accidental position is mistaken by the algorithm for that of the signal peak. Most runaways showed either a low correlation value when compared with the rest of the particles, or a missing clear distinction between highest peak and next highest peak. In addition, the size of the shift vector was used as a criterion for rejection. Particles that have been windowed out with the aid of the interactive selection program are known to be centered within ± 5 image elements in either direction. Deviations larger than ± 10 units from the true center in either direction would already result in a partial truncation of the particle. Shift vectors outside of a square box with side length 10 units around the center are therefore definitely due to a false correlation peak. These criteria could in principle be used to identify and exclude misaligned particles in a completely automatic run of the program.

Figure 7 shows the averages of 50 negatively stained molecules imaged with low, medium, and high dose and those of 20 glucose/stain treated molecules with low and high dose. Column A shows the sixfold rotationally symmetrized averages directly displayed without any additional contrast stretching. Column B shows the same averages after application of the density-stretching procedure, resulting in an enhanced display of the stain-excluding regions of the averaged molecule. Column C shows density-stretched averages before they have been rotationally symmetrized. Columns D and E contain the glucose/stain averages before and after symmetrization. All averages show the presence of sixfold symmetry. Comparison of independent partial averages, here shown for the

---

Fig. 6. a) A typical cross-correlation function of a GS particle with the reference particle. The position of the peak with respect to the origin (center of frame) indicates the relative position of the particles with respect to each other. b) Section through the cross-correlation function as indicated in Figure 6a. c) Eight particles before (top row) and after (bottom row) alignment. The first particle on the left was used as reference. Note that in the four corners of each aligned particle image there appear incursions of the image average as a result of the rotations and circular shifts applied by the computer.

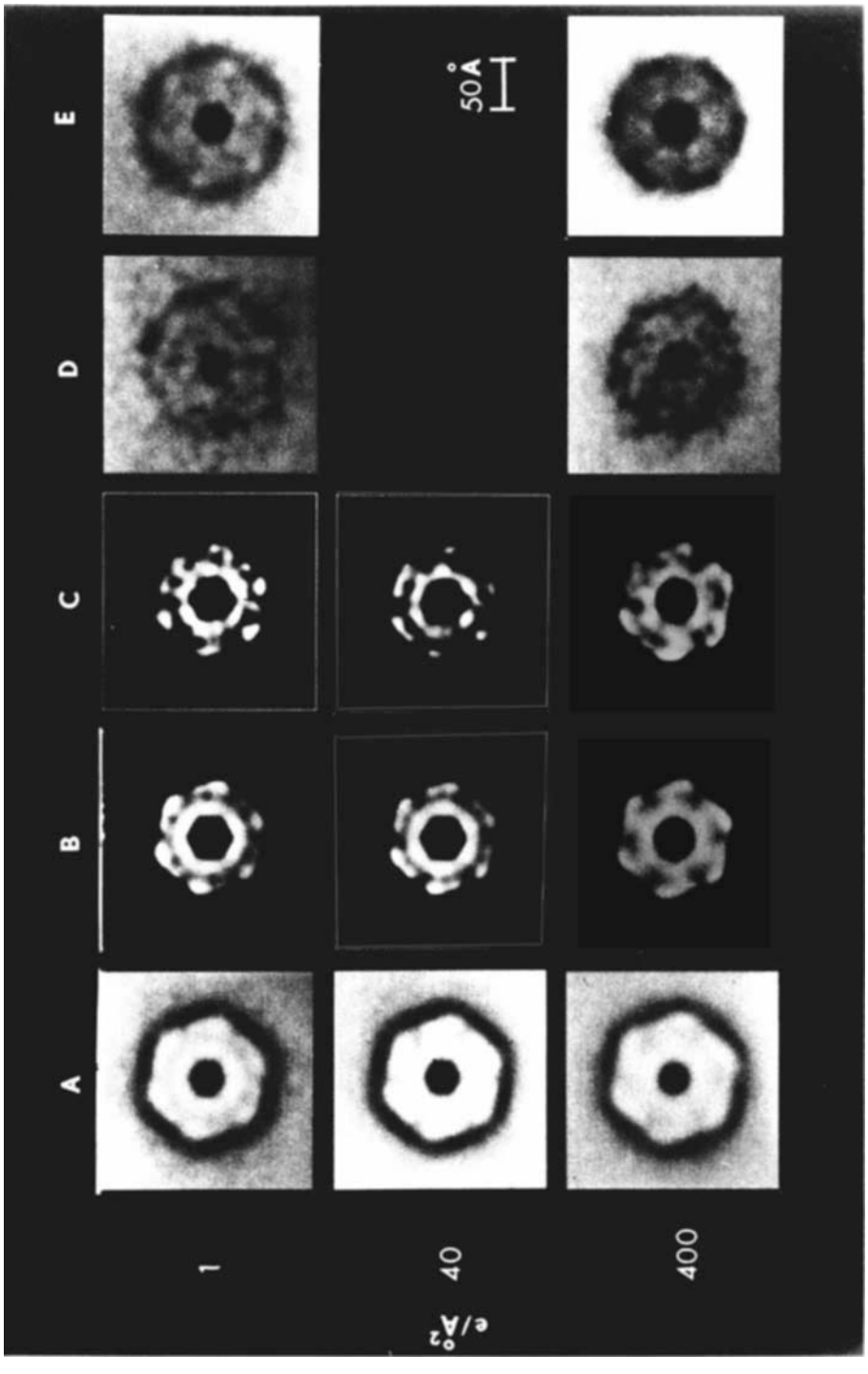

Fig. 7. Half-tone representation of the molecule averages obtained for low, medium and high electron dose. No medium dose images were available for the glucose/uranyl acetate treated specimen. Column A) Direct displays of sixfold rotationally symmetrized averages obtained with negative staining (uranyl formate). Column B) Same as A, only stain-excluding region shown with enhanced contrast. Only the upper third of the optical density range is seen, expanded into the full density range of the filmwriting. The molecule particle appears isolated with sharp outer and inner boundaries produced by the threshold. Column C) Same as B before sixfold rotational symmetrization. Column D) Direct displays of averages obtained with glucose/uranyl acetate staining. Column E) Same as D after sixfold rotational symmetrization.

low dose average of negatively stained molecules (Fig. 8), proves that the main features visible in the reconstruction are reproducible: 1) skewed arrangement of subunit domains, producing pinwheel appearance of the molecule projection; 2) radial division of the subunit domains into two domains. A display of the Fourier transform (Fig. 9) shows the presence of sixfold symmetry out to 1/23 $Å^{-1}$ in the case of the low dose average of negatively stained glutamine synthetase and 1/28 $Å^{-1}$ in the corresponding high dose average. In contrast to this, the range of symmetry is hard to define in power spectra of glucose/stain-treated molecules, probably owing to the fact that the relatively small number of molecules (20) used for the nonsymmetrized average does not suppress the noise spectrum sufficiently. For the representations of all averages, we used Gaussian low-pass filtering with a radius at 1/18 $Å^{-1}$.

DISCUSSION

As in the results described by Frank et al [8], the averages of the negatively stained particles show a marked handedness similar to a pinwheel, which can be explained by the assumption of preferential contrasting of one of the hexamers by the stain.

We have investigated the stain behavior with additional experiments. We made tilt series of the specimen in order to find other evidence for the partial staining of the hexamer. Upon tilting, the projections of the stain-excluding regions change their shape in the same manner as those of an entirely flat disk. This is true both for the particles that rest on their end and those that rest on their side. The end-on particles shorten in the direction normal to the tilt axis by an amount characteristic of a flat disk rather than lengthen as would be expected from the tilted view of a fully stained cylindrical particle with diameter 137 Å and height 80 Å. Also, the edges of the stain-excluding area do not change their appearance to show the sides of the molecule. Similarly, molecules lying on their side with their axes normal to the tilt axis show no indication of their end faces at tilts greater than 45°. With regard to the question of preferential staining, these results are, however, inconclusive, because the molecules are apparently severely flattened in the staining and drying process. This is evidenced by the fact that particles surrounded by heavy stain concentrations are about 20% smaller in diameter than those more lightly stained which were used in the reconstructions. The heavy stain restricts the flattening. This can be seen in the tilted views.

The pinwheel appearance of the projection of a single hexamer is in agreement with the results of Frey [7], who obtained patterns with cyclic symmetry and alternate handedness in successive z-sections of the central strand in a three-dimensional reconstruction of a negatively stained 6 + 1 glutamine synthetase cable.

For a detailed discussion of the results, we use contour representations of the sixfold rotationally symmetrized averages. Figure 10 shows the average of the negatively stained molecules as compared with that of molecules treated with the glucose/stain mixture under different dose conditions.

Even in the case of low dose conditions, the maxima visible in the interior stain-excluding region are two or three times larger than the noise fluctuations outside of the molecule, and can therefore be considered significant in terms of structural interpretation at the 20 Å level.

In the images of the negatively stained molecule we can recognize an almost circular region with an approximately 50 Å diameter as marked on the contour plot of the low dose average. According to the low resolution reconstruction of Frey [7], the

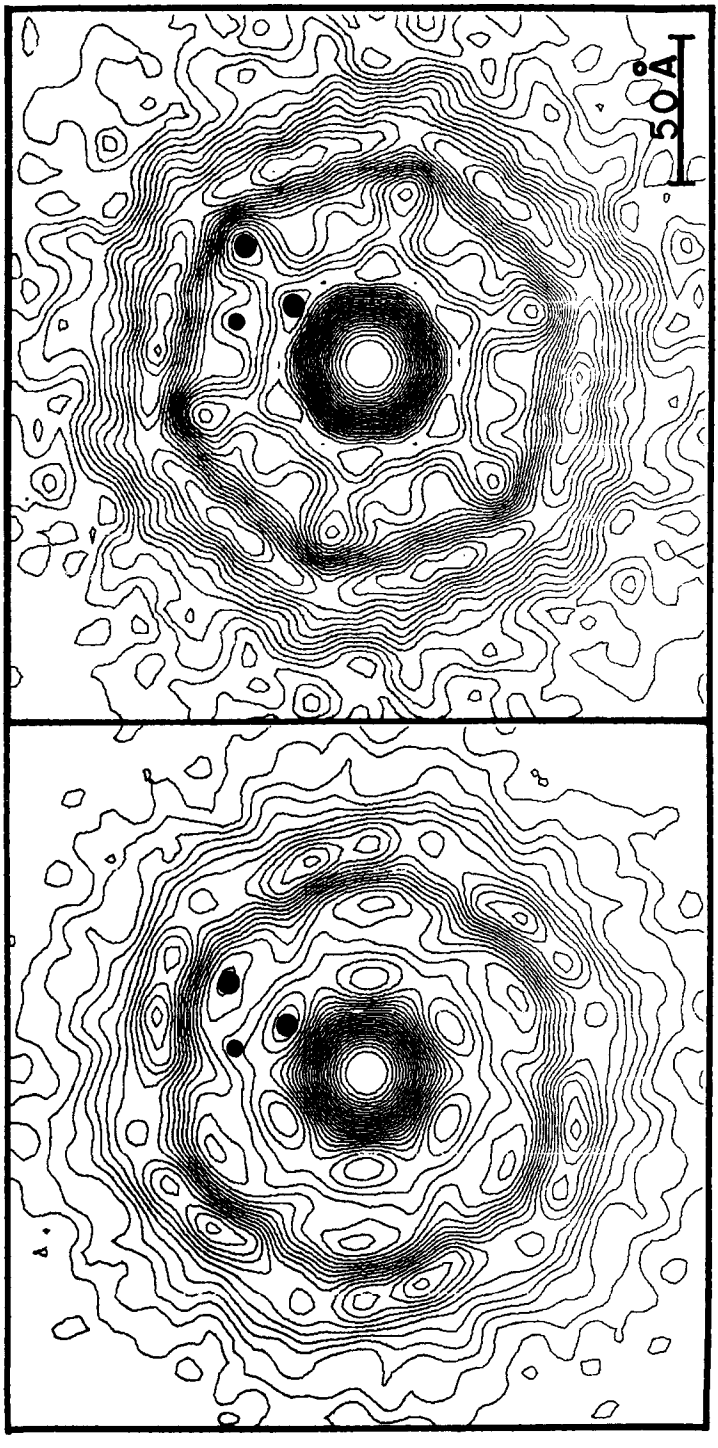

Fig. 8. Rotationally symmetrized averages of two independent particle sets, each consisting of 25 stained, low dose particle images obtained with negative staining. The comparison of the contour plots shows the extent of reproducibility of the averaging method. In both averages, the subunit domains appear skewed with respect to the particle radius and divided radially into two subdomains (centers marked by big dots). A smaller domain appears on the left-hand side of the outer subdomain (marked by small dot) but this is stronger expressed in the average on the right-hand side.

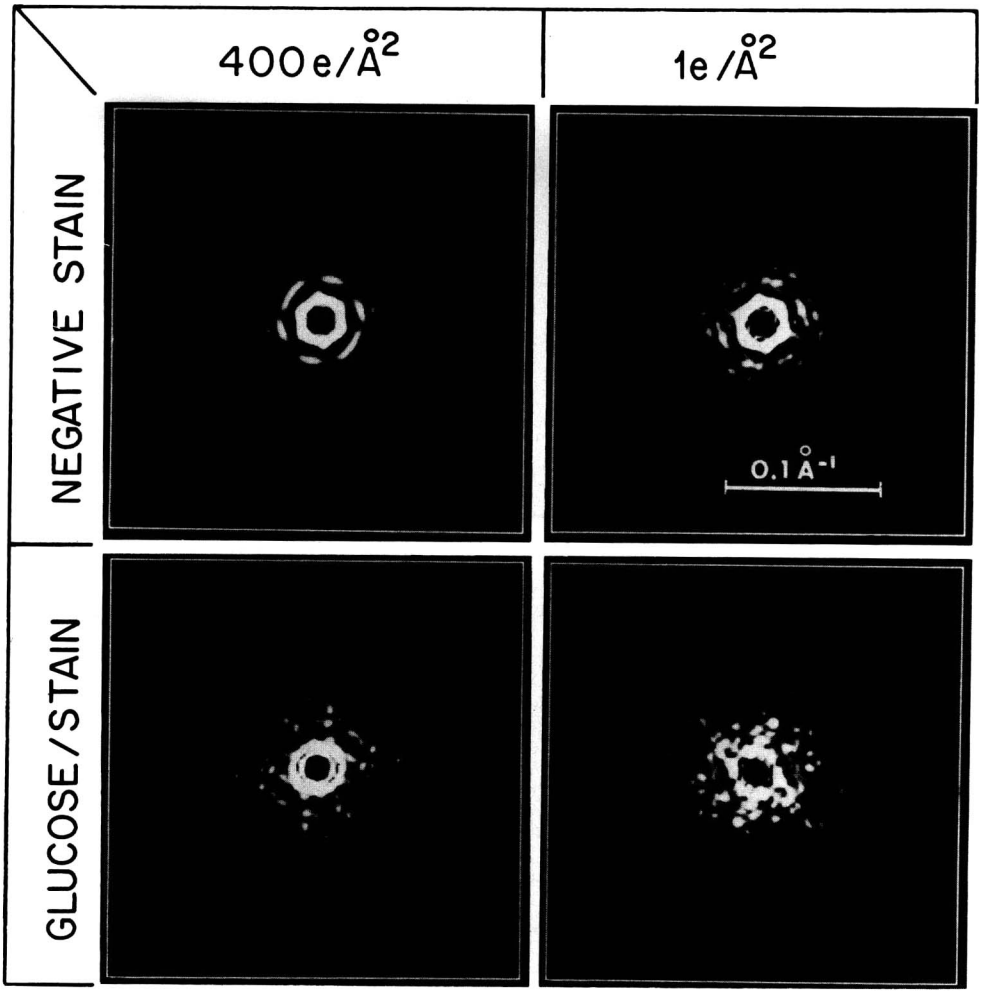

Fig. 9. Fourier transforms of the averages before rotational averaging, showing sixfold symmetry preserved to various resolutions. The central area with high Fourier intensity was removed by masking, in order to bring out the high resolution components of the transform more clearly.

individual subunit has a circular shape with a 63 Å diameter when viewed in axial projection. We can explain our results by assuming that we see the projection of two eclipsed subunits of asymmetric shape. The deviation from mirror symmetry, visible as a distinct handedness of the projection, may be explained by the difference in staining between bottom and top hexamer. Such a difference would mainly affect the appearance of the noneclipsed part of the subunit.

In the low dose negatively stained average we can distinguish one inner and one outer major density peak and a third outer subsidiary peak within the projection of the eclipsed subunit pair. The groove apparently penetrated by the stain lies between the outermost major peak and the weaker peak to its left, and leads into a region of low density dividing the inner from the outer major peak. The groove and its continuation form a division between a major inner part of the subunit and a minor outer part. This

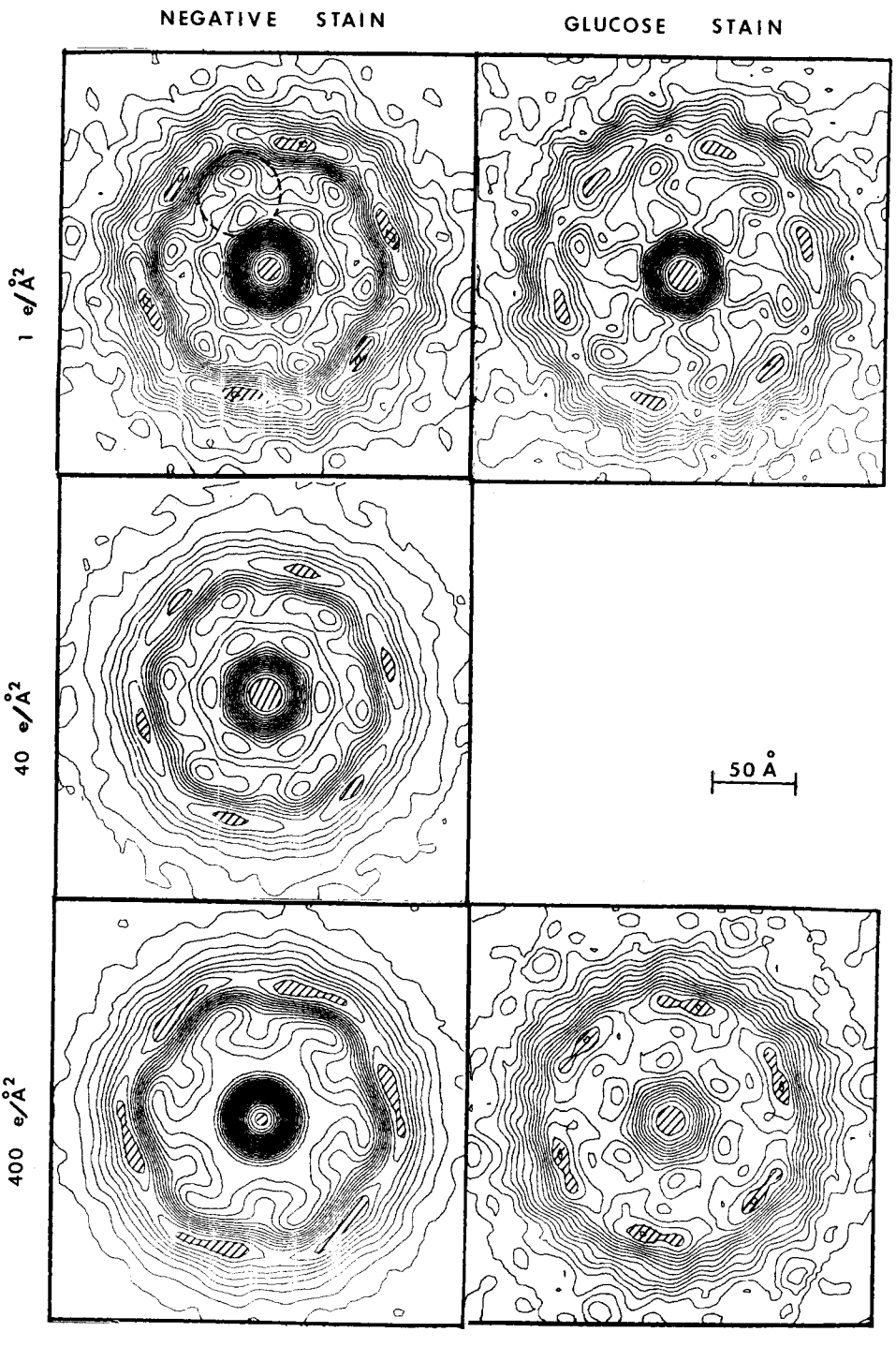

Fig 10. Contour representations of the averages. Left column: negatively stained molecules; right column: glucose/stain treated molecules. The contour maxima due to stain concentrations are marked by shading.

would be a logical proteolytically sensitive region along which the splitting off of the 18k fragment from the subunit in the limited proteolysis experiment of Lei et al [2] occurs. In this case the cleavable fragment would correspond to the outer high density peak. A volume ratio of 18:32 would be visible as an area ratio of 1:1.5 in projection if we assume spherical shapes for the fragments. This ratio is consistent with the size ratio of the observed subunit regions in the low dose average.

In the medium and high dose averages we can see that the outer subsidiary peak is the first density region to disappear as the electron dosage increases. In the high dose average only the outer major peak has remained as a defined region within the subunit. From the evidence presented we can point to a specific sequence of events as a function of the increase in electron dosage. The main phenomenon appears to be a migration of the stain from its original location in the fine groove separating the two domains of the subunits, and hence effectively reducing the attainable resolution. A similar behavior of negative stain has been reported by Unwin [24] in the case of stacked disks of TMV. Evidence of such resolution loss is found in the display of the Fourier transforms for high and low dose (Fig. 8).

The main structural features visible in the low dose stain average are reproduced by the low dose glucose/stain reconstruction. The glucose/stain shows, however, additional positive staining effects. The protein is more heavily stained than the background area between particles, and the stain meniscus that borders the particle is relatively more concentrated in the area between the subunits. The glucose/stain preparation is very radiation-sensitive when compared to the ordinary negative stain preparation. This can be seen from the loss of visible sixfold symmetry and other details in the high dose reconstruction. The only remnant of subunit detail present in the high dose average is the density peak adjacent to the central core.

CONCLUSIONS

The results of this paper naturally lead to the question of how much farther the technique can be pushed toward higher resolution and more explicit structural interpretability. Earlier theoretical studies showed that a resolution of 7 Å is feasible in principle [22]. The resolution of 23 Å deduced from the symmetry of the power spectrum is consistent with the expected limitation due to the structure of negative stain. The use of the glucose/stain mixture brought no improvement, neither in resolution nor interpretability. The realization of significantly higher resolution will require the use of an embedding medium which contrasts the particle yet does not interfere with the interpretation of the protein distribution. An alternative is the use of a noncontrasting embedding medium such as glucose in conjunction with a procedure for locating the particle in a separate experiment.

A higher resolution average of a single projection such as we have here would, however, probably be difficult to interpret because of the overlapping of details. In order for a higher resolution reconstruction to yield more useable information about the molecule, we must combine three-dimensional reconstruction from tilted views with the low dose averaging procedure (cf [8]). The observed flattening of protein dried on a carbon film must be overcome if a three-dimensional reconstruction is to be meaningful. Freeze-drying or critical-point-drying may accomplish this.

ACKNOWLEDGMENTS

We would like to thank Dr. F. Wedler for a gift of the glutamine synthetase preparation, and acknowledge helpful discussions with Dr. F. Wedler and Dr. D. Eisenberg. We would like to thank Kurt Asmus for his help with microscopy, scanning, and film-writing, and Helen Dowse for assistance with the image processing.

REFERENCES

1. Tyler B: Ann Rev Niochem 47:1127, 1978.
2. Lei M, Aebi U, Heidner EG, Eisenberg D: J Biol Chem 254:3129, 1979.
3. Valentine RC, Shapiro BM, Stadtman ER: Biochemistry 7:2143, 1968.
4. Kabsch W, Kabsch H, Eisenberg DS: J Mol Biol 100:283, 1976.
5. Eisenberg DS, Heidner EG, Goodkin P, Dastor MN, Weber BH, Wedler F, Bell JD: Cold Spring Harbor Sympos Quant Biol 36:291, 1971.
6. Frey TG, Eisenberg DS, Eisenberg FA: Proc Natl Acad Sci USA 72:3402, 1975.
7. Frey T: Proc 9th Intl Congr El Microsc Toronto, 1978, vol III, p 107.
8. Frank J, Goldfarb W, Eisenberg D, Baker TS: Ultramicroscopy 3:283, 1978.
9. Frank J, Goldfarb W, Eisenberg D, Baker TS: Ultramicroscopy 4:247, 1979.
10. Frank J, Goldfarb W, Kessel M, Eisenberg D, Baker TS: Biophys J 21:89a, 1978.
11. Frank J, Goldfarb W, Kessel M: Proc 9th Intl Congr El Microsc Toronto, 1978, vol II, p 8.
12. Kessel M, Frank J, Goldfarb W: In Baumeister W (ed): "Electron Microscopy in Molecular Dimensions. State of the Art and Strategies for the Future." Heidelberg: Springer-Verlad, 1980.
13. Shapiro BM, Stadtman ER: In Perlman GE, Lorand L (eds): "Methods in Enzymology." New York: Academic Press, 1970, vol XIX, p 910.
14. Unwin PNT, Henderson R: J Mol Biol 94:425, 1975.
15. Henderson R, Capaldi RA, Leigh JS: J Mol Biol 112:631, 1977.
16. Turner JN, Hausner GG, Parsons DF: J Phys E: Sci Instr 8:954, 1975.
17. Smith PR, Aebi U, Josephs R, Kessel M: J Mol Biol 106:243, 1976.
18. Frank J, Shimkin B: Proc 9th Intl Congr El Microsc Toronto, 1978, vol I, p 210.
19. Frank J: Proc 9th Intl Congr El Microsc Toronto, 1978, vol III, p 87.
20. Goldfarb W, Frank J: Proc 9th Intl Congr El Microsc Toronto, 1978, vol II, p 22.
21. Kuo I, Glaeser RM: Ultramicroscopy 1:55, 1975.
22. Saxton WO, Frank J: Ultramicroscopy 2:219, 1977.
23. Welles K: In Bailey GW (ed): Proc 33rd Ann EMSA Mtg Las Vegas. Baton Rouge, Louisiana: Claitor's Publishing Co, 1975.
24. Unwin PNT: J Mol Biol 87:657, 1974.